Power law observed in the motion of an asymmetric camphor boat under viscous conditions

Michiko Shimokawa,* Masashi Oho, and Kengo Tokuda
Fukuoka Institute of Technology, 3-30-1 Wajiro-Higashi, Higashi-ku, Fukuoka 811-0295, Japan

Hiroyuki Kitahata
Department of Physics, Chiba University, Yayoi-cho 1-33, Inage-ku, Chiba 263-8522, Japan

(Received 20 March 2018; revised manuscript received 3 August 2018; published 29 August 2018)

We investigated the velocity of an asymmetric camphor boat moving on aqueous solutions with glycerol. The viscosity was controlled by using several concentrations of glycerol into the solution. The velocity decreased with an increase in the glycerol concentration. We proposed a phenomenological model, and we showed that the velocity decreased with an increase in the viscosity according to power law. Our experimental result agreed with the one obtained from our model. These results suggest that a decay length of the camphor concentration at the front side of the boat is sufficiently shorter than that of the rear side.

DOI: 10.1103/PhysRevE.98.022606

I. INTRODUCTION

We can observe a wide variety of patterns, such as in a traffic jam [1–3], a large-scale ordering of swimming bacteria [4,5], a swarm of mosquitoes, a parliament of birds, and a school of fish [6–8], formed by living things as self-propelled objects. It is one of the challenges of understanding pattern formations induced by these collective motions.

Similar behaviors also emerge in chemical systems, such as microtubes [9], droplets [10–12], Janus particles [13,14], and camphor systems [15–31]. Self-propelled objects transform chemical energy into kinetic energy in nonequilibrium systems, and they move spontaneously as if they were living. Recently, a lot of studies have reported on camphor boats as self-propelled particles in the chemical system [15–20]. A camphor boat is made of a plastic sheet attached to a camphor disk. When the camphor boat is put on an aqueous surface, the camphor molecules dissolve from the disk under the boat and expand on the surface. As the camphor molecules decrease the surface tension of the aqueous phase, the camphor boat moves on the aqueous phase spontaneously due to a difference in surface tension around the boat. There have been many experimental studies, as well as numerical ones, on the camphor boat. Some of the numerical models are based on reaction-diffusion dynamics on the camphor concentration [20–24], and the others are based on fluid dynamics [25–27]. These models could explain the experimental behaviors in a qualitative manner. Basic physical quantities were necessary in order to realize the quantitative correspondence. However, it had been difficult to measure the driving force on the motion of the camphor boat, the surface tension difference between the front and the back of the boat, the diffusion coefficient, the supply rate of camphor molecules from the camphor disk to the water surface, and a relaxation rate before Suematsu *et al.* measured these quantitative properties in experiments [18]. The results have allowed us to compare the experimental results with theoretical ones quantitatively, and they have provided a deep understanding of the interesting phenomena of the camphor boat. However, they investigated only the situation for pure water as an aqueous phase. Thus, we focused on the viscosity dependence of the motion with regard to a camphor boat.

As methods to change the viscosities of the aqueous solution under the camphor boat, temperature control of the solution or the use of the solution with different physical concentration is considered. We adopted the latter; we used aqueous solutions of glycerol with several glycerol concentrations [21,28], and we changed the viscosity of the base solution.

In this paper, we investigated the velocity v of the camphor boat for several glycerol concentrations p, and we found that v decreased with an increase in p. To understand the p dependence of v, we proposed the mathematical model. The model showed a power law $v \sim \mu^{-1/2}$, where μ is the viscosity of the base solution. Our experimental results satisfied the scaling relation obtained from the mathematical model. The agreement between the experimental result and the theoretical result for the viscosity dependence of v provides an estimation of the concentration field around the camphor boat, which is difficult to measure directly in experiments.

II. EXPERIMENTAL PROCEDURE

A round-shape boat as shown in Figs. 1(a) and 1(b) was used to measure the velocity of the camphor boat. The boat was composed of a plastic plate (thickness: 0.1 mm) and a camphor disk, which was prepared by pressing camphor powder [(+)-Camphor, Wako, Japan] using a pellet die set for the preparation of samples on Fourier-transform–infrared (FT-IR) spectroscopy analysis. The diameter and the thickness of the camphor disk were 3.0 and 1.0 mm, respectively. The plastic plate was cut in a circle with a diameter of 6.0 mm, and the camphor disk was attached to the edge of the flat circular plastic plate using an adhesive (Bath bond Q, KONISHI, Japan), so that half of the camphor disk was outside of the plastic sheet. This round-shape camphor boat moved toward the direction of the plastic sheet.

*Corresponding author: shimokawa@fit.ac.jp

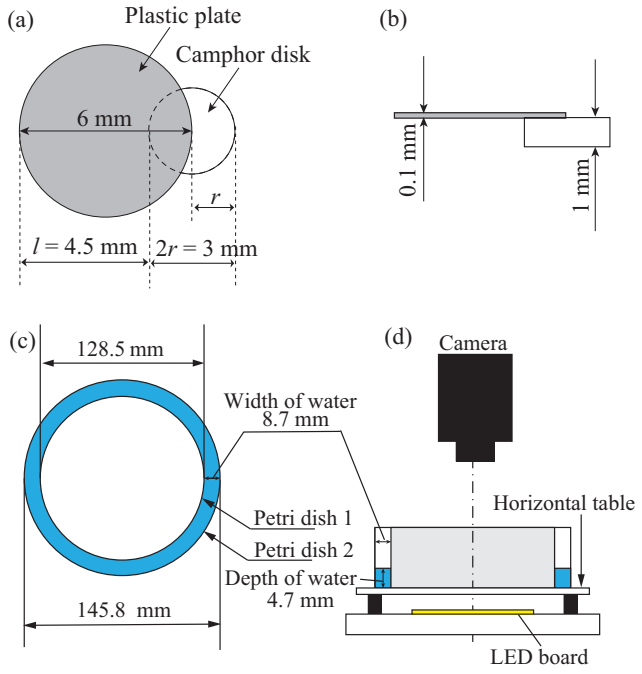

FIG. 1. Schematic drawings of (a) top view and (b) side view of a camphor boat for the measurements of velocities, (c) top view, and (d) side view on the annular chamber.

An annular glass chamber was used, which was composed of two petri dishes with different diameters as shown in Figs. 1(c) and 1(d). Inner and outer diameters were 128.5 and 145.8 mm, and the channel width of the chamber was thus 8.7 mm. As it is known that the velocity is sensitive to the depth of water [19], the chamber was put on a clear horizontal plate. The solution was poured into the chamber so that the depth of the solution was 4.7 mm; the solution was glycerol (Glycerol, Wako, Japan) and water mixed at several mass ratios p, i.e., p is a percentage of a glycerol mass in the mixed solution. We investigated the physical properties of the solution, such as the viscosity, the surface tension, and the camphor solubility against glycerol concentration p. The detailed results are shown in Appendix A. The camphor boat was put on the surface of the solution in the glass chamber, and then it started to move spontaneously. For a visualization of the motion, a LED board was placed under the horizontal plate. The motion of the boat was captured with a digital video camera (HDR-FX1, SONY, Japan) from the top of the chamber. Obtained movies were analyzed using an image-processing system (ImageJ, Nature Institutes of Health, USA).

III. EXPERIMENTAL RESULTS

We investigated the velocity of the camphor boat on the solutions of various glycerol concentrations p. The position of the camphor boat is described as a radial angle θ in the annular chamber, as shown in Fig. 2(a). Analyses of the videos captured by the digital video camera provide the position θ at time t, where $t = 0$ corresponds to the time when the boat finished three laps along the chamber after the boat had been put on the surface of the solution. In Fig. 2(b), θ had a constant gradient in time, that is to say, the camphor boat moved with a constant velocity. Figure 2(c) shows a time series of the angular velocity $\omega = \Delta\theta/\Delta t$, where $\Delta t = 1/30$ s for one frame of the video camera and $\Delta\theta$ is an angular difference between t and $t + \Delta t$. In Fig. 2(b), the expanded plot is shown for the time region corresponding to the gray region in Fig. 2(c). The angular velocity ω in the region fluctuated around the average value 1.08 rad/s. A similar tendency was observed at $50 \lesssim t \lesssim 200$ s, i.e., ω increased with time and had noisy data before $t \sim 10$ s, and ω began to decrease after $t \sim 250$ s. Therefore, we investigated ω at $60 \lesssim t \lesssim 180$ s, during which ω had almost a constant value for time. Next, we investigated the angular velocity for p as shown in Fig. 2(d). The vertical and horizontal axes in Fig. 2(d) show the angular velocity $\overline{\omega}$ and concentration p. The $\overline{\omega}$ was obtained from the linear fitting of time series as shown in Fig. 2(b). The values of the errors for each $\overline{\omega}$ were lower than 10^{-3} rad/s. As shown in Fig. 2(d), $\overline{\omega}$ decreased with an increase in p.

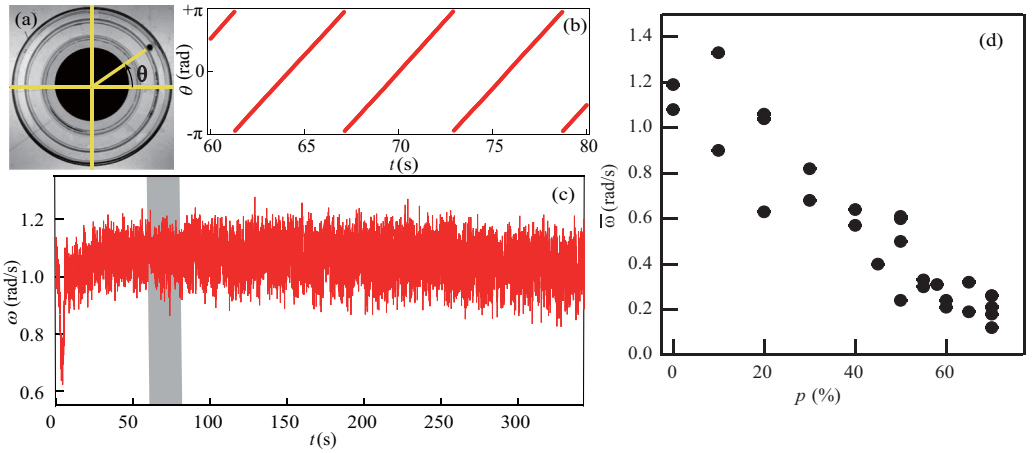

FIG. 2. (a) Snapshot of the camphor boat motion. (b) Time series of the position θ of a camphor boat moving on water ($p = 0$), where θ is the angle shown in (a). (c) Time series of angular velocity ω of the camphor boat, where $\omega = \Delta\theta/\Delta t$ for each frame. The gray region corresponds to the time range shown in (b). (d) Dependence of $\overline{\omega}$ on p, where p is the glycerol concentration and $\overline{\omega}$ is the angular velocity obtained from linear fitting of time series as shown in (b).

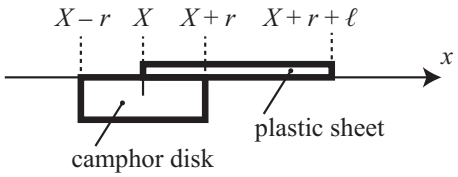

FIG. 3. Illustration of the side view of a camphor boat.

IV. MATHEMATICAL MODEL

The glycerol concentration p of the solution was controlled in our experiments, which led to a change in the viscosity μ shown in Appendix A. In this section, we consider a viscosity dependence of the camphor boat velocity. Now, the annular glass chamber used in our experiments is recognized as a one-dimensional channel with an infinite length.

The time evolution equation of the camphor boat in a one-dimensional system (the spatial coordinate is represented as x) is given as

$$m\frac{d^2X}{dt^2} = -h\frac{dX}{dt} + F, \tag{1}$$

where m, X, h, and F are the mass, the center of mass, the friction coefficient of the camphor boat, and the driving force exerted on the moving camphor boat, respectively. We assume that h is proportional to viscosity μ such as $h = K\mu$, where K is a constant ($K > 0$). The assumption has been used in many previous papers [15–18,20–25,28], and it was also reported that the viscous drag on the mobility of thin film in Newtonian fluid obeyed a linear relationship with the fluid viscosity [32]. Therefore, we considered that the assumption $h = K\mu$ is natural [33]. The driving force F is described as

$$F = w\{\gamma[c(X + r + \ell)] - \gamma[c(X - r)]\}, \tag{2}$$

where w is the width of the camphor disk. Here, we consider that the positions of the front and the back of the boat are shown as $x = X + r + \ell$ and $x = X - r$, where r and ℓ are the radius of the disk and the size of the boat as defined in Fig. 3. The surface tension γ depends on the concentration c of the camphor molecules at the surface of the solution, and we assume the linear relation as

$$\gamma = \gamma_0 - \Gamma c, \tag{3}$$

where γ_0 is the surface tension of the base solution without camphor and Γ is a positive constant.

The time evolution on the camphor concentration c is shown as

$$\frac{\partial c}{\partial t} = D\frac{\partial^2 c}{\partial x^2} - ac + f(x - X), \tag{4}$$

where a is the sum of sublimation rate and dissolution rate of the camphor molecules on the solution surface, D is the diffusion coefficient of the camphor molecule, and f denotes the dissolution rate of the camphor molecules from the camphor disk to the aqueous solution surface. As for the term $f(z)$, we apply the following description:

$$f(z) = \begin{cases} f_0 & (-r < z < r), \\ 0 & (\text{otherwise}). \end{cases} \tag{5}$$

That is to say, the dissolution of camphor molecules from the disk occurs at $-r < z < r$. The above equation does not include the Marangoni effect directly, although the flow has an influence on the camphor concentration. Reference [31] showed that Eq. (4) was reasonable if D was recognized as the spatially uniform effective diffusion coefficient of the camphor to include the transportation by the flow. In addition, this spatially uniform effective diffusion coefficient is supported by the experimental results that the diffusion length is proportional to the square root of elapsed time [15].

V. THEORETICAL ANALYSIS

Our experimental results showed that the camphor boat moved with a constant velocity in time, as shown in Fig. 2. Thus, we should consider solutions for the motion of the camphor boat with a constant velocity v in the x direction, i.e., $X = vt$. From this condition, Eq. (1) leads to

$$-hv + F = 0. \tag{6}$$

By setting $\xi = x - vt$ and $c = c(\xi)$, Eq. (4) provides

$$-v\frac{dc}{d\xi} = D\frac{d^2c}{d\xi^2} - ac + f(\xi). \tag{7}$$

Equation (7) leads to the following solutions:

$$c(\xi) = \begin{cases} \beta_1 \exp[\lambda_-(\xi - r)] & (\xi > r), \\ \frac{f_0}{a} + \alpha_2 \exp(\lambda_+\xi) + \beta_2 \exp(\lambda_-\xi) & (-r < \xi < r), \\ \alpha_3 \exp[\lambda_+(\xi + r)] & (\xi < -r), \end{cases} \tag{8}$$

where

$$\lambda_\pm = -\frac{v}{2D} \pm \frac{\sqrt{v^2 + 4Da}}{2D}, \tag{9}$$

$$\beta_1 = \frac{f_0\lambda_+}{a(\lambda_+ - \lambda_-)}[1 - \exp(2\lambda_- r)], \tag{10}$$

$$\alpha_2 = \frac{f_0\lambda_- \exp(-\lambda_+ r)}{a(\lambda_+ - \lambda_-)}, \tag{11}$$

$$\beta_2 = -\frac{f_0\lambda_+ \exp(\lambda_- r)}{a(\lambda_+ - \lambda_-)}, \tag{12}$$

$$\alpha_3 = -\frac{f_0\lambda_-}{a(\lambda_+ - \lambda_-)}[1 - \exp(-2\lambda_+ r)]. \tag{13}$$

Equations (8)–(13) provide

$$\begin{aligned} F &= -\Gamma w[\beta_1 \exp(\lambda_-\ell) - \alpha_3] \\ &= -\frac{\Gamma w f_0}{a(\lambda_+ - \lambda_-)}\{\lambda_+[1 - \exp(2\lambda_- r)]\exp(\lambda_-\ell) \\ &\quad + \lambda_-[1 - \exp(-2\lambda_+ r)]\}. \end{aligned} \tag{14}$$

As v is sufficiently large in our experiments, we assume $r \ll 1/\lambda_+$ and $\ell \gg 1/|\lambda_-|$. Then, $\lambda_+ \sim a/v$ and $\lambda_- \sim -v/D$, which lead to

$$\begin{aligned} F = -\frac{\Gamma w f_0}{a(v/D)}\left\{\frac{a}{v}\left[1 - \exp\left(-\frac{2vr}{D}\right)\right]\exp\left(-\frac{v}{D}\ell\right)\right. \\ \left. - \frac{v}{D}\left[1 - \exp\left(-\frac{2ar}{v}\right)\right]\right\} \end{aligned}$$

$$\simeq -\frac{\Gamma w f_0 D}{av}\left(-\frac{v}{D}\right)\left(\frac{2ar}{v}\right)$$
$$= \frac{2\Gamma w f_0 r}{v}. \tag{15}$$

As $F = K\mu v$ from Eq. (6),

$$K\mu v = \frac{2\Gamma w f_0 r}{v}. \tag{16}$$

From Eq. (16), we obtain

$$v = \sqrt{\frac{2\Gamma w f_0 r}{K\mu}}. \tag{17}$$

Equation (17) shows a power law $v \propto \mu^{-1/2}$ if other parameters such as Γ, w, and f_0 are independent of μ. The power law with the index $-1/2$ is an interesting result, since the Stokes relation naturally suggests another relation, $v \propto \mu^{-1}$ [34].

VI. NUMERICAL RESULTS

In the theoretical analysis, we have assumed the solution depending on $\xi = x - vt$. However, the supposed mathematical model has other symmetries, and whether the considered solution depending on ξ is an attractor or not should be checked. Therefore, we performed numerical calculations based on equations in Sec. IV. For numerical calculation, we considered a one-dimensional array with a spatial step of $\Delta x = 0.1$. The spatial size of the considered system was 1000 with a periodic boundary condition, and we adopted the Euler method with time step $\Delta t = 10^{-3}$. As for the spatial derivative, we used an explicit method. The parameters are set to be $m = 0.1$, $w = 1$, $\Gamma = 1$, $r = 1$, $\ell = 1$, $D = 1$, $a = 1$, and $f_0 = 1$. In the discretization process, the first-order interpolation was adopted for Eqs. (2) and (5). The parameter h corresponding to the viscosity μ was changed, and we investigated the time development of the camphor boat position and camphor concentration profile.

In Fig. 4, the numerical results are shown. In Fig. 4(a), the time development of camphor boat velocity is shown. The camphor boat velocity is saturated to a constant value. The camphor concentration profile after the velocity became constant ($t = 1000$) is shown in Fig. 4(b). The camphor concentration profile was asymmetric with regard to the camphor boat position $x = X \simeq 188.6$. After reaching a constant velocity, the concentration profile did not change the shape but shifted in a positive x direction. Thus, we can guess that the solution with regard to $\xi = x - vt$ is an attractor of this system. We have also confirmed that the solution converged to this attractor from other initial conditions (data not shown). The mathematical analysis on this convergence to the solution depending on ξ remains, and it may be possible to approach such a mathematical problem by considering Lie group symmetry [35].

The final velocity against h is shown in Fig. 4(c). For the regime of h smaller than 0.1, the power law $v \propto h^{-1/2}$ held, where h was proportional to the viscosity μ in the present framework. In the theoretical analysis, we assumed $r \ll 1/\lambda_+$ and $\ell \gg 1/|\lambda_-|$, which is equivalent to $aD/v^2 \ll 1$, as will be discussed in detail in the following section. Since the final velocity is nearly equal to 5 for $h \sim 0.1$, and $a = D = 1$, the divergence from the power law originates from the breakdown of the assumption in the analysis.

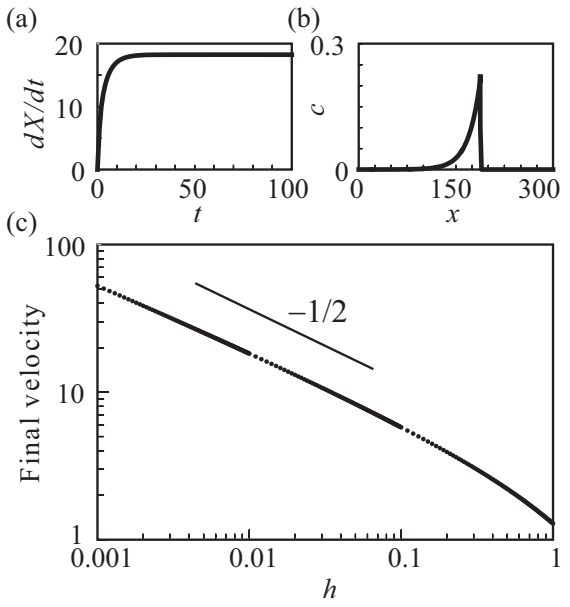

FIG. 4. Numerical results. (a) Time course of camphor boat velocity dX/dt for $h = 0.01$. (b) Camphor concentration profile $c(x)$ for $h = 0.01$ at $t = 1000$, when the camphor boat velocity reached a constant value. The position of the camphor boat was $X \simeq 188.6$. (c) Final velocity ($t = 1000$) depending on h, which is proportional to viscosity. The power law $v \propto h^{-1/2}$ holds for smaller h.

VII. DISCUSSION

Our model showed a power law $v \sim \mu^{-1/2}$ under the assumptions that $r \ll 1/\lambda_+$ and $\ell \gg 1/|\lambda_-|$. In this section, we compare experimental results with the numerical results in Eq. (17) in order to check whether our model is reasonable. Equation (17) has several parameters, such as Γ, w, f_0, r, K, and μ. Since similar camphor boats were used, w, r, and K were constant values in our experiments. We investigated the dependence of the other parameters, i.e., Γ, f_0, and μ, on the glycerol concentration p in Appendix A. Equation (3) showed $\Gamma = (\gamma_0 - \gamma)/c$. As $(\gamma_0 - \gamma)$ was independent of p in our measurements, we considered that Γ was constant. The supply rate f_0 corresponds to ΔM, which is a loss of a camphor disk per unit time in our experiments, and we found that ΔM decreased with an increase in p. The viscosity μ of the base solution increased with p. Thus, f_0 and μ in Eq. (17) are functions of p. In addition, the angular velocity is proportional to the camphor boat velocity in our experiments.

From the above discussion, Eq. (17) leads to

$$\overline{\omega}(p) \propto \sqrt{\frac{\Delta M(p)}{\mu(p)}}. \tag{18}$$

Figure 5 shows a relationship between $\Delta M/\mu$ and $\overline{\omega}$ obtained from our experiments. The result almost agrees with the solid line in Eq. (18) [36].

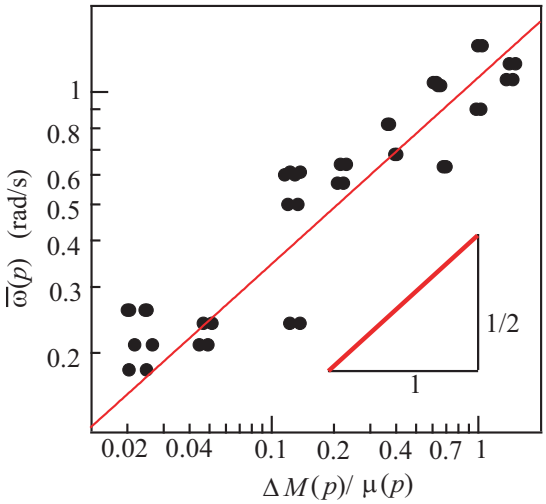

FIG. 5. Relationship between $\Delta M/\mu$ and $\overline{\omega}$, where ΔM, μ, and $\overline{\omega}$ are the weight loss of a camphor disk per one second, the viscosity of the base solution, and the angular velocity of the camphor boat, respectively. The solid line shows the numerical result; $\overline{\omega} \sim \sqrt{\Delta M/\mu}$ in Eq. (18).

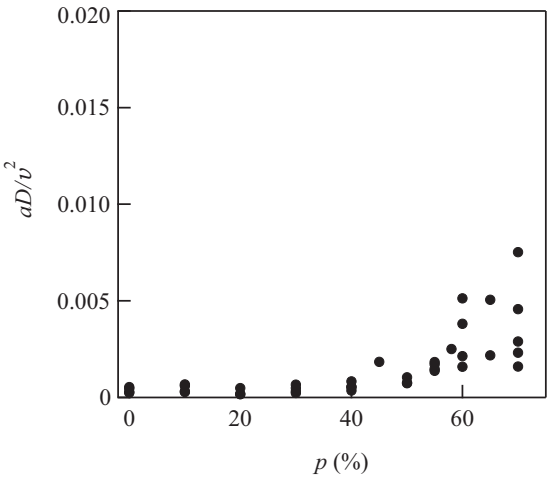

FIG. 6. Relationship between p and aD/v^2, where a, D, and v correspond to the sum of sublimation rate and dissolution rate of camphor molecules on an aqueous surface, effective diffusion coefficient, and velocity of a camphor boat, respectively. aD/v^2 was much smaller than 1, which suggests our approximation is valid.

The power law was obtained under the assumptions that $r \ll 1/\lambda_+$ and $\ell \gg 1/|\lambda_-|$, which is equivalent to $aD/v^2 \ll 1$. Since $\sqrt{D/a}$ corresponds to a characteristic decay length of the camphor concentration profile, and v/a is a distance of the camphor boat motion during the characteristic time during which the concentration field keeps the memory, the assumption means that the characteristic length for the camphor concentration profile is sufficiently smaller than the characteristic length for the camphor boat motion. In such a case, the camphor concentration profile should be asymmetric with respect to the camphor particle position.

Here, we confirm the acceptability of the assumptions for our experiments. We needed values of parameters such as a, D, and v included in the assumption. We used a rectangular camphor boat and chalk powders in measurements of D. The boat was put on the solution surface covered by the chalk powders, and the camphor diffused into the solution. The diffusion was visualized by the chalk powders. We analyzed the videos of the powders' motion and estimated D. The method of the measurement is similar to that in a previous study [18]. The effective diffusion coefficient D against p is shown in Appendix B, which shows that D decreases with an increase in p. For a, $a = 1.8 \times 10^{-2}\ \mathrm{s}^{-1}$ was used, which was based on the experimental observation reported in the previous work [18]. Using these data, the relationship between p and aD/v^2 was obtained as shown in Fig. 6. The result shows that the values of aD/v^2 were sufficiently smaller than 1 for all p, which suggests that our assumption is reasonable. The result provides the following consideration: the camphor concentration around the boat is quite asymmetric, and the decay length of the concentration field at the back of the boat is sufficiently greater than that at the front.

There have been many analytical studies on collective motion of symmetric camphor disks in both experiments and theoretical analyses [16,22,23,30]. There have also been some studies on asymmetric camphor boats, in which numerical calculation for both concentration field and camphor boat positions was performed, and an analytical approach under the assumption of slow velocity was performed [15,24]. In contrast to these studies, we operated under the assumption of fast velocity, and this assumption was justified by the experimental observation. It would enable an analytical approach on the collective motions of the camphor boats with fast velocity. Therefore, our model would provide a deep understanding of the collective motions on not only camphor boats but also living things.

VIII. CONCLUSION

We investigated the velocity v of the asymmetric camphor boat against several glycerol concentrations p of the glycerol aqueous solution. To know the dependence of the camphor boat velocity v on the glycerol concentration p, we discussed a numerical model based on a diffusion-reaction equation. When it is assumed that the characteristic length of the camphor concentration at the front of the boat is shorter than that at the rear, v should obey a power law $v \sim \mu^{-1/2}$, where μ is the viscosity of the base solution. The power law agreed with experimental results, and it was also confirmed that our assumption in the model was reasonable through a comparison with our experimental results. Using our proposed model, we can discuss the profile of camphor concentration, which is difficult to measure directly in experiments. Thus, our experiment has profound significance in the estimation of the concentration through the measurements of the velocity.

As a future topic, it would be worth investigating whether a similar power law $v \sim \mu^{-1/2}$ persists with smaller levels of v in experiments with such variables as an increased boat size. In addition, we considered that the hydrodynamic effect was included in the effective diffusion coefficient in this paper. However, it would also be important to consider the fluid flow around the boat when we study the behavior of two or more camphor boats as the collective motion. As future work,

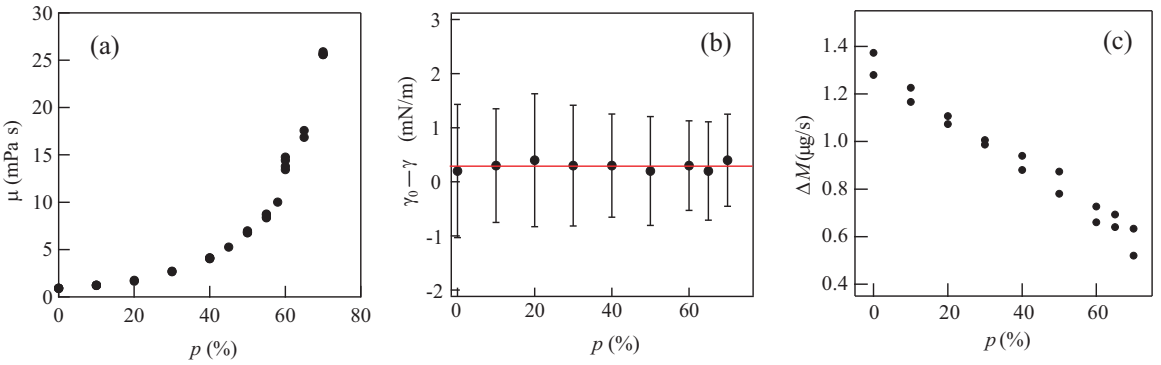

FIG. 7. Physical properties of aqueous solutions of glycerol as the base solution. (a) Viscosity μ against glycerol concentration p, which is a percentage of glycerol mass in a glycerol-water solution. (b) Surface tension difference $\gamma_0 - \gamma$ against p, where γ_0 and γ are the surface tension of a glycerol-water solution without camphor molecules and that of the solution in which camphor molecules are dissolved, respectively. (c) Weight loss ΔM against p.

it would also be interesting to consider the hydrodynamic interaction in a multiple-camphor-particle system.

ACKNOWLEDGMENTS

This work was supported by Y. Koyano. M.S. would like to thank Samantha Hawkins of Fukuoka Institute of Technology for proofreading this manuscript. This work was supported by JSPS KAKENHI Grants No. JP18K11338, No. JP18K03572, No. JP25103008, and No. JP15K05199.

APPENDIX A: PHYSICAL PROPERTIES OF A GLYCEROL-WATER SOLUTION AS A BASE SOLUTION

Figure 7(a) shows a viscosity dependence for various glycerol concentrations p of the aqueous solution; i.e., p means a percentage of a glycerol mass in the aqueous solution. The viscosity μ was measured using a viscometer (SV-10A, A&D, Japan). As shown in Fig. 7(a), the viscosity μ increased with p.

Figure 7(b) shows a surface tension difference $\gamma_0 - \gamma$ of the solution for p, where γ_0 and γ correspond to the surface tension for a glycerol-water solution without camphor and that for the solution with 6.8×10^{-3} g camphor dissolved per 1500 mL, respectively. The camphor concentration was set to become close to that in measurements of angular velocity ω. The surface tension was measured using a surface tensiometer (DMs-401, Kyowa Interface Science Co., Ltd., Japan). The surface tension γ with camphor was lower than that of γ_0 without the camphor, and γ and γ_0 decreased with an increase in glycerol concentration p. The difference of $\gamma - \gamma_0$, however, almost remained constant for different values of p as shown in Fig. 7(b). The average value of $\gamma - \gamma_0$ was 0.29 mN/m.

Next, we investigated the dependence of camphor solubility on the glycerol concentration p of the base solution. We measured the mass of the camphor disk before and after the camphor disk moved for $\Delta t = 50$ min, and the mass change was set to be ΔM. From ΔM, we obtained the weight loss rate $\Delta M = \Delta m/\Delta t$. As shown in Fig. 7(c), ΔM decreased with an increase in p.

APPENDIX B: EFFECTIVE DIFFUSION COEFFICIENT OF CAMPHOR ON A SOLUTION WITH SEVERAL GLYCEROL CONCENTRATIONS

The effective diffusion coefficient D of camphor is included in our assumption, and the value of D was necessary for checking whether the assumption was reasonable. Thus, we measured D for various glycerol concentrations p.

The rectangular boat in Figs. 8(a)–8(b) was used for the measurements of the effective diffusion coefficient of the camphor molecules on the solution, and its shape was different from the round-shaped boat in the measurements of the velocity.

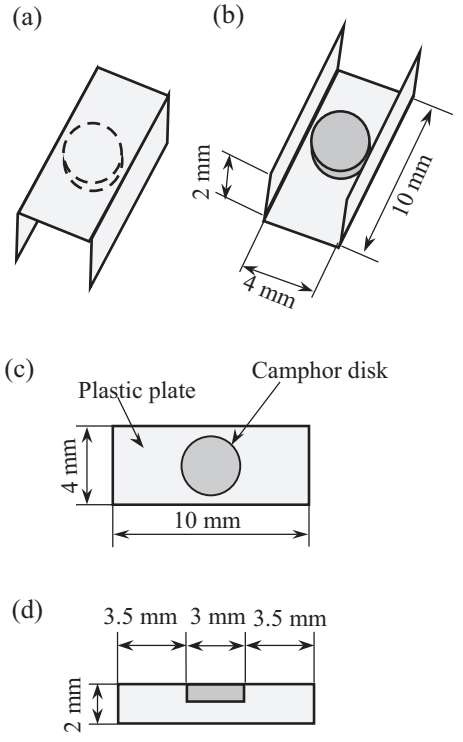

FIG. 8. Schematic drawings of (a) three-dimensional view, (b) upside-down three-dimensional view, (c) top view, and (d) side view of a camphor boat used for the measurements of effective diffusion coefficients.

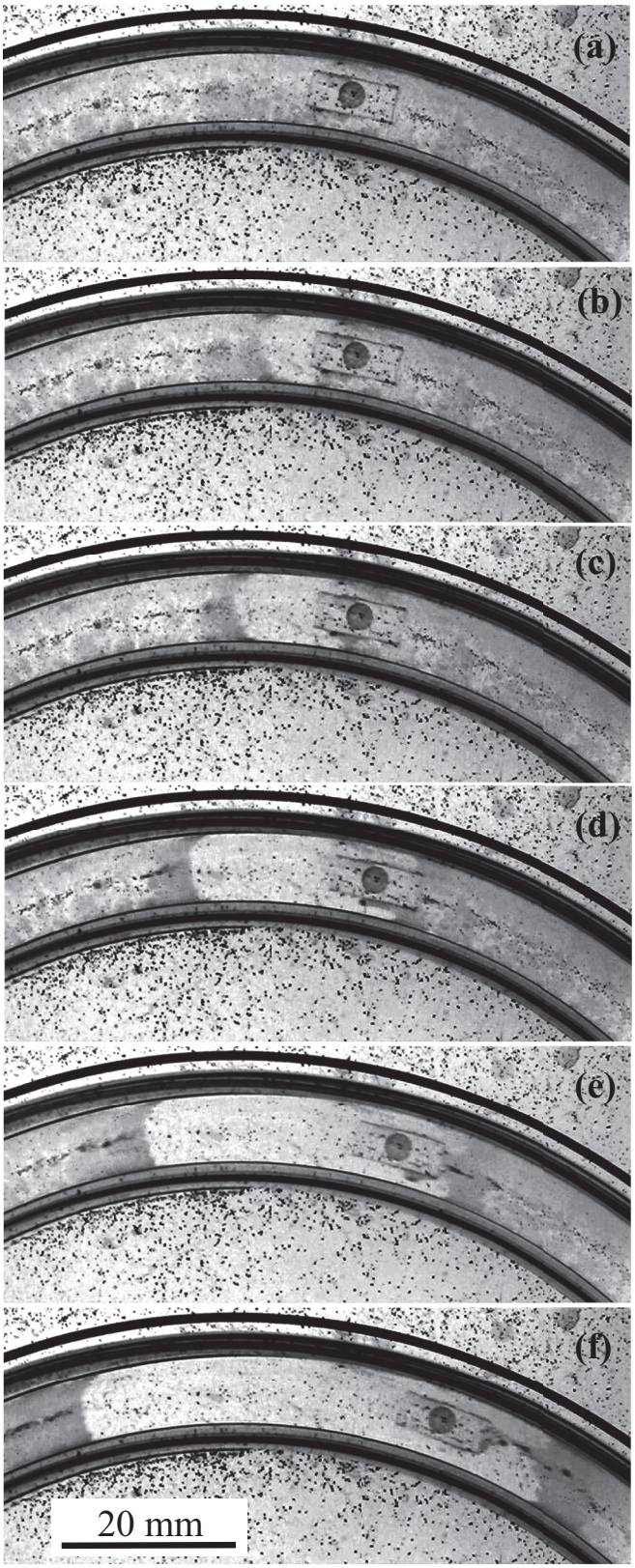

FIG. 9. Snapshots on the expansion of the camphor molecular layer at (a) $t = 0$ s, (b) 0.03 s, (c) 0.07 s, (d) 0.13 s, (e) 0.20 s, and (f) 0.30 s, respectively. Chalk powders were dispersed on the solution surface for visualization of the camphor layer. The white and gray regions indicate the camphor layer and the region rich in floating chalk powders, respectively.

The rectangular boat was made by bending both sides of a rectangular plastic plate that was 8.0 mm in width and 10.0 mm in height at 2.0 mm from the edge. The camphor disk was attached at the center of the plastic plate, where the shortest distance from the edge was 3.5 mm. The shape was similar to the one reported in a previous study [18].

Figures 9(a)–9(f) are snapshots captured from the top at time t, where (a) $t = 0$ s, (b) 0.03 s, (c) 0.07 s, (d) 0.13 s, (e) 0.20 s, and (f) 0.30 s, respectively. In Fig. 9, $t = 0$ corresponds to the time at which the chalk powders started moving on the water. The diffusion of camphor molecules under the rectangular boat leads to the motion of chalk powders on the water surface. As shown in Fig. 9(a), all regions of the surface were covered by chalk powders with a gray color at $t = 0$. The chalk powders started moving at $t = 0.03$ s, and the water surface without powders was observed as a white region around the boat

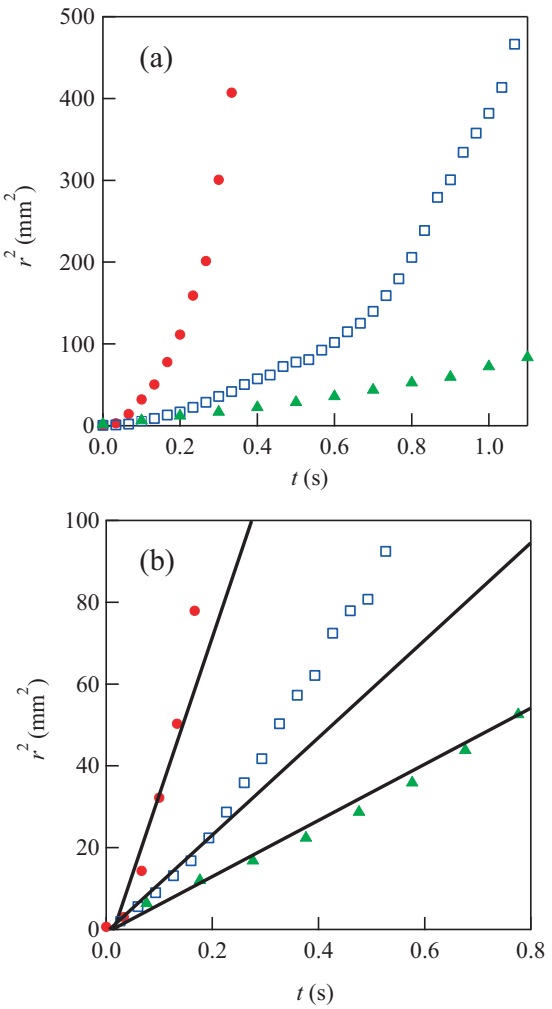

FIG. 10. (a) Relationship between time t and r^2, where r is the longest distance between the edge and the center of the area from which chalk powders were swept out. $t = 0$ corresponds to the time at which chalk powders on the solution started moving. Closed circles, open squares, and closed triangles show the data for glycerol concentrations $p = 0\%$ ($\mu = 0.92$ mPa s), $p = 40\%$ ($\mu = 4.03$ mPa s), and $p = 70\%$ ($\mu = 25.80$ mPa s), respectively. (b) An expanded one for $0 < t < 0.8$ s in (a), and solid lines are the results of the linear fittings for time before the boat started moving.

in Fig. 9(b). The area of the white region grew with time [Figs. 9(b)–9(d)]. The boat stayed at the same position before $t \sim 0.2$ s [Figs. 9(a)–9(e)], although the powders moved. The camphor boat, then, started to move after $t \sim 0.2$ s [Fig. 9(f)]. In this process, the chalk powders were carried by not only the camphor diffusion but also fluid flow induced by the motion of the boat.

Next, we investigated r^2 at time t, where r was the longest distance between the edge and the center of the region with the camphor layer, shown as the white region in Fig. 9. The closed circles, open squares, and closed triangles in Fig. 10(a) show the data for $p = 0\%$ ($\mu = 0.92$ mPa s) for water, and $p = 40\%$ ($\mu = 4.03$ mPa s) and $p = 70\%$ ($\mu = 25.80$ mPa s) for the glycerol-water solution, respectively. Let us focus on the data for $p = 0$. The trend of the data changed around at $t \sim 0.2$ s, which almost corresponded to the time when the camphor boat began to move, as shown in Fig. 9. As we needed the effective diffusion coefficient of the camphor, we measured r^2 in the time range in which the camphor boat did not move. Figure 10(b) is an expanded figure for small t, i.e., time without the boat motion. When the camphor boat stayed at a certain position, r^2 increased linearly with time. Linear fittings are shown as solid lines, where fitting was executed for the region $0 < t < 0.13$ s for closed circles. The gradients of these solid lines provide the effective diffusion coefficients D of the camphor molecules on the glycerol-water solution. The effective diffusion coefficient on the water was obtained at 180 ($\pm$ 20) mm^2/s. A previous paper [31] reported that the effective diffusion coefficient D in a numerical study almost agreed with the value for D measured with this method. Thus, we consider that this method is reasonable for the measurement of D. The gradient of the solid line decreases with an increase in the glycerol concentration. Figure 11 shows the relationship between p and D, and the tendency that D decreases with an increase in p was confirmed.

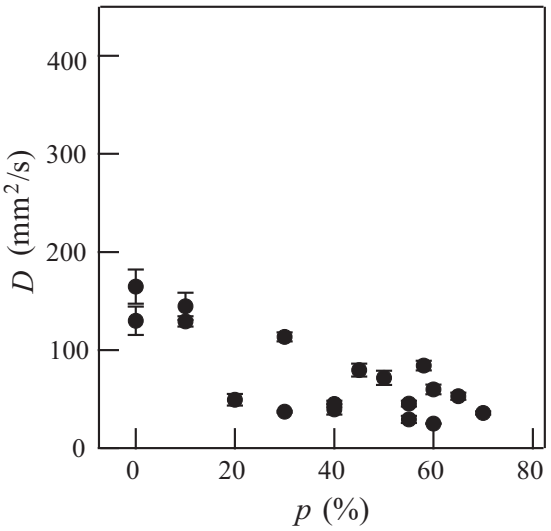

FIG. 11. Effective diffusion coefficient D against glycerol concentrations p of the base solutions. Error bars denote standard deviations.

[1] A. Nakayama *et al.*, New J. Phys. **11**, 083025 (2009).
[2] M. Bando, K. Hasebe, K. Nakanishi, and A. Nakayama, Phys. Rev. E **58**, 5429 (1998).
[3] Y. Sugiyama *et al.*, New J. Phys. **10**, 033001 (2008).
[4] C. Peng *et al.*, Science **354**, 882 (2016).
[5] D. Nishiguchi, K. H. Nagai, H. Chaté, and M. Sano, Phys. Rev. E **95**, 020601(R) (2017).
[6] T. Vicsek, A. Czirók, E. Ben-Jacob, I. Cohen, and O. Shochet, Phys. Rev. Lett. **75**, 1226 (1995).
[7] T. Vicsek and A. Zafeiris, Phys. Rep. **517**, 71 (2012).
[8] J. Toner and Y. Tu, Phys. Rev. Lett. **75**, 4326 (1995).
[9] Y. Sumino *et al.*, Nature (London) **483**, 448 (2012).
[10] S. Thutupalli, R. Seemann, and S. Herminghaus, New J. Phys. **13**, 073021 (2011).
[11] T. Ohmura *et al.*, Appl. Phys. Lett. **107**, 074102 (2015).
[12] S. Tanaka, S. Nakata, and T. Kano, J. Phys. Soc. Jpn. **86**, 101004 (2017).
[13] D. Nishiguchi *et al.*, New J. Phys. **20**, 015002 (2018).
[14] J. Hu *et al.*, Chem. Soc. Rev. **41**, 4356 (2012).
[15] N. J. Suematsu, S. Nakata, A. Awazu, and H. Nishimori, Phys. Rev. E **81**, 056210 (2010).
[16] H. Nishimori, N. J. Suematsu, and S. Nakata, J. Phys. Soc. Jpn. **86**, 101012 (2017).
[17] M. I. Kohira *et al.*, Langmuir **17**, 7124 (2001).
[18] N. J. Suematsu *et al.*, Langmuir **30**, 8101 (2014).
[19] Y. Matsuda *et al.*, Chem. Phys. Lett. **654**, 92 (2016).
[20] S. Nakata *et al.*, Phys. Chem. Chem. Phys. **17**, 10326 (2015).
[21] M. Nagayama *et al.*, Physica D **194**, 151 (2004).
[22] E. Heisler *et al.*, J. Phys. Soc. Jpn. **81**, 074605 (2012).
[23] K. Nishi *et al.*, Phys. Rev. E **92**, 022910 (2015).
[24] E. Heisler *et al.*, Phys. Rev. E **85**, 055201(R) (2012).
[25] S. Soh, K. J. M. Bishop, and B. A. Grzybowski, J. Phys. Chem. B **112**, 10848 (2008).
[26] S. Soh, M. Branicki, and B. A. Grzybowski, J. Phys. Chem. Lett. **2**, 770 (2011).
[27] E. Lauga and A. M. J. Davis, J. Fluid Mech. **705**, 120 (2011).
[28] Y. Koyano, T. Sakurai, and H. Kitahata, Phys. Rev. E **94**, 042215 (2016).
[29] N. J. Suematsu *et al.*, J. Phys. Soc. Jpn. **84**, 034802 (2015).
[30] Y. S. Ikura *et al.*, Phys. Rev. E **88**, 012911 (2013).
[31] H. Kitahata and N. Yoshinaga, J. Chem. Phys. **148**, 134906 (2018).
[32] H. A. Stone and H. Masoud, J. Fluid Mech. **781**, 494 (2015).
[33] It would be interesting to investigate the viscous dependence for a viscous drag directly in a similar experiment to Ref. [18].
[34] J. Happel and H. Brenner, *Low Reynolds Number Hydrodynamics: With Special Applications to Particulate Media* (Springer, Netherlands, 1983).
[35] P. J. Olver, *Applications of Lie Groups to Differential Equations* (Springer, New York, 1993).
[36] The experimental data are distributed since the values of ΔM are noisy, as shown in Fig. 7(c). The values of ΔM, investigated in the motion of the camphor disk, are sufficiently small to be susceptible to external factors.